Supermodes in Coupled Multi-Core Waveguide Structures

Cen Xia, M. Amin Eftekhar, Rodrigo Amezcua Correa, Jose Enrique Antonio-Lopez, Axel Schülzgen, Demetrios Christodoulides, and Guifang Li, *Fellow, IEEE*

(Invited Paper)

***Abstract*—Optical supermode dynamics are nowadays receiving an ever increasing attention in mode-division multiplexing applications. In this paper, we systematically analyze and characterize these modes in various structures based on coupled-mode theory. In particular, we investigate the structure of supermodes in honeycomb multi-ring arrangements of any size. In addition, we show that higher order supermodes in coupled few-mode multi-core waveguide arrays can be strongly affected by angle-dependent couplings, leading to different modal field profiles. Analytical solutions are provided for linear, rectangular, and ring arrays. Higher order supermodes are observed for the first time in a coupled few-mode three-core fiber system using the S^2 imaging method.**

***Index Terms*—Microstructure, optical waveguides, optical fibers, optical fiber communication, space division multiplexing.**

I. Introduction

SUPERMODES are eigenmodes of composite structures involving coupled constituent elements, each of which also supporting guided modes in isolation [1], [2]. As indicated in a number of studies, such multi-core systems can be effectively analyzed using coupled-mode theory (CMT)—which is particularly effective when the coupling between neighboring elements is relatively weak. Over the years, the properties of supermodes in either linear [3] or ring arrays of coupled waveguides have been analyzed using CMT methods [4]–[6]. Even in the simplest possible configuration of two coupled channels, supermodes play an important role given that their interference is the one responsible for the energy exchange behavior in a directional coupler.

Quite recently, supermodes have received renewed interest within the context of mode-division multiplexing (MDM), a new transmission method aimed at overcoming the capacity limit of single-mode fiber communication systems. Since modes tend to couple during long-distance fiber transmission, unravelling mode crosstalk using multiple-input-multiple-output (MIMO) digital signal processing (DSP) is necessary for demultiplexing MDM channels [7]. In the presence of modal group dispersion, the computational load for MIMO DSP is proportional to the modal group delay [8]. Interestingly, coupled multi-core fibers can be designed to have reduced modal group delays and/or larger effective areas in comparison with few-mode fibers (FMF) [9]. In a recent experiment, the modal delay was also found to depend sublinearly on transmission distance in the presence of strong supermode coupling [10]. It is thus imperative to study the properties of optical supermodes in a systematic manner. Such study can help predict the mode behavior in various coupled multi-core waveguides, including single-mode or few-mode coupled multi-core fibers [10], [11], directional couplers or the slow-tapering regime of the multi-core lanterns [12], [13].

In this paper, we analyze and characterize the modes of multi-core structures that could be potentially useful in MDM systems. For structures with single mode constituent elements, we investigate, in Section II, supermode arrangements in multi-ring honeycomb lattices. Supermode structures with multimode constituent elements were first introduced in [14]. In Section III, we provide analytical description for higher-order supermodes in such array configurations, including linear, ring and square array lattices. Finally in Section IV, we present an experimental observation of higher-order supermodes in a 3-core fiber array.

II. Supermodes in Multi-Ring Honeycomb Structures

Honeycomb waveguide arrangements have been intensely investigated over the years [15]–[22]. Their close-packed geometry makes them ideal for multi-core fiber application. In this section, we develop a general methodology capable of analyzing supermodes in multi-ring honeycomb waveguide lattices, consisting of any number of layers. In addition to hexagonal systems, this versatile technique can be used in other regular polygonal configurations. In brief, our approach is based on separately formulating an eigenvalue problem for in-phase supermodes and another for modes with orbital angular momentum. This can be achieved by appropriately grouping the constituent waveguide elements based on their topology. Here, this approach is explicitly demonstrated in honeycomb arrangements involving 7, 19, and 37 sites.

We begin our analysis by assuming that in all cases, each waveguide element is assumed to be cylindrical (of radius a) and single-moded, i.e., it only supports the LP_{01} mode, with a propagation constant β_0. The coupling coefficient κ between waveguide channels can then be obtained using coupled-mode

Manuscript received June 14, 2015; revised August 30, 2015; accepted September 1, 2015. This work was supported in part by the National Basic Research Program of China (973) Project #2014CB340104/1, NSFC Projects 61377076, 61307085, and 61431009, and the United States Army Research Office grant W911NF-13-1-0283.

C. Xia, M. A. Eftekhar, R. A. Correa, J. E. Antonio-Lopez, A. Schülzgen, and D. Christodoulides are with the CREOL, The College of Optics and Photonics, University of Central Florida, Orlando FL 32816 USA (e-mail: cxia@creol.ucf.edu; m.a.eftekhar@Knights.ucf.edu; r.amezcua@creol.ucf.edu; jealopez@creol.ucf.edu; axel@creol.ucf.edu; demetri@creol.ucf.edu).

G. Li is with the The College of Precision Instrument and Optoelectronic Engineering, Tianjin University, Tianjin 300072, China (e-mail: li@creol.ucf.edu).

Color versions of one or more of the figures in this paper are available online at http://ieeexplore.ieee.org.

Digital Object Identifier 10.1109/JSTQE.2015.2479158

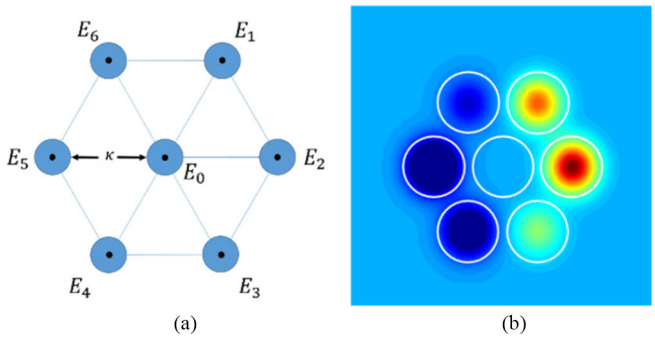

Fig. 1. (a) A 7-core hexagonal lattice. All single mode waveguide elements interact with their nearest neighbors with a coupling strengthκ. (b) Real part of the field distribution($\sim \cos(Qn)$)associated with the DS_{11} supermode.

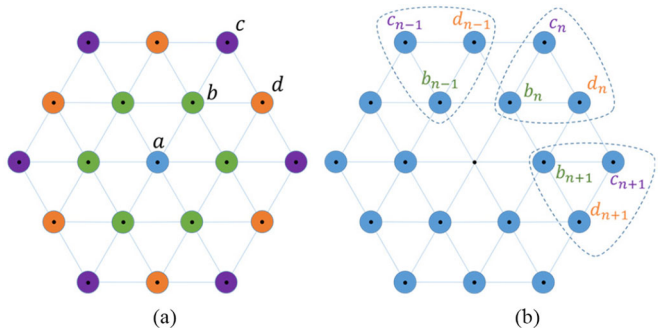

Fig. 2. (a) A 19-core hexagonal lattice. The waveguide elements are grouped in four different families (a, b, c, d) indicated with different colors. (b) By excluding the central core, the remaining elements of these families are in addition grouped in each hexagonal sector in order to obtain supermodes having angular momenta.

theory. If the distance between core centers, i.e., the core pitch is D, this coupling strength is given by [23], [24]:

$$\kappa = \frac{\sqrt{2\Delta}}{a}\frac{U^2}{V^3}\frac{K_0(WD/a)}{K_1^2(W)} \tag{2.1}$$

where $\Delta = (n_c - n_s)/n_c$ is the waveguide index difference and n_c, n_s are the core and cladding refractive indices, respectively. $V = k_0 a n_c\sqrt{2\Delta}$ is the dimensionless V number involved in the eigenvalue problem describing the fundamental mode LP_{01} of the waveguide, e.g., $UJ_1(U)/J_0(U) = WK_1(W)/K_0(W)$. In the last equation, $U = a\left(k_0^2 n_c^2 - \beta^2\right)^{1/2}$, $W = a\left(\beta^2 - k_0^2 n_s^2\right)^{1/2}$, where $K_l(x)$ and $J_l(x)$ are Bessel functions of order l. The propagation constant β can be determined from the eigenvalue problem by keeping in mind that $V^2 = U^2 + W^2$.

In this section, we will exemplify our method in the case of a 7-, 19-, and 37-core hexagonal lattice. Even though both the 7- and 19-core systems have been previously analyzed using either direct schemes or linear algebraic methods [18], [21], [22], here we will still apply our methodology to these same geometries for demonstration purposes.

A 7-core arrangement is shown in Fig. 1(a). In this multi-core system the modal fields evolve according to:

$$i\frac{dU_0}{dz} + \beta_0 U_0 + \kappa\sum_{n=1}^{6} U_n = 0 \tag{2.2a}$$

$$i\frac{dU_n}{dz} + \beta_0 U_n + \kappa U_0 + \kappa(U_{n+1} + U_{n-1}) = 0. \tag{2.2b}$$

In Eq. (2.2) we only account for nearest neighbor interactions in this hexagonal system. By introducing a gauge transformation $U_n = u_n \exp(i\beta_0 z)$ and by adopting a dimensionless coordinate $Z = \kappa z$ one arrives at

$$i\frac{du_0}{dZ} + \sum_{n=1}^{6} u_n = 0 \tag{2.3a}$$

$$i\frac{du_n}{dZ} + u_0 + (u_{n+1} + u_{n-1}) = 0. \tag{2.3b}$$

In all cases, the modes can be re-expressed in terms of actual quantities and coordinates in a straightforward fashion. In solving this problem, we look for discrete supermodes, henceforth denoted as DS_{lm}, where the discrete index l represents an orbital angular momentum and m is the root number of the corresponding eigenvalue equation. To obtain the seven supermodes of the structure depicted in Fig. 1(a), we first seek in-phase modes of the type DS_{0m} that represent to some extent discrete analogues to the continuous LP_{0m} modes in standard cylindrical waveguides [24, 25]. Under this assumption and by exploiting the symmetry of this problem, one can identify two species, u_a, u_b where $u_a = u_0$ and $u_b = u_1 = u_2 = \ldots = u_6$. From Eq. (2.3) we find that $idu_a/dZ + 6u_b = 0$ and $idu_b/dZ + 2u_b + u_a = 0$. To obtain the dispersion relation of these in-phase modes we assume solutions of the type $u_a = u_a^0 e^{i\lambda Z}$ and $u_b = u_b^0 e^{i\lambda Z}$ that directly lead to an algebraic eigenvalue equation for the normalized propagation constant λ,$\lambda^2 - 2\lambda - 6 = 0$, with solutions $\lambda = 1 \pm \sqrt{7}$. As we will see these two eigenvalues correspond to the two in-phase supermodes DS_{01} and DS_{02}. From here, the eigenvectors $[u_a^0, u_b^0]$ can be readily deduced from the corresponding eigenvalue problem.

We next consider supermodes involving angular momentum. In this respect, the modal fields in the outer ring vary according to $u_n = Be^{i\lambda Z}e^{iQn}$. In addition, we assume that the field in the central element is zero ($u_0 = 0$). In this case

$$i\frac{du_n}{dZ} + u_{n+1} + u_{n-1} = 0. \tag{2.4}$$

Given that any solution of this latter equation must repeat itself after six elements, (e.g., $6Q = 2l\pi$), then upon substitution of u_n in Eq. (2.4) we deduce that

$$\lambda = 2\cos(Q) \tag{2.5}$$

where $Q = l\pi/3$ and the angular momentum index takes values from the set $l = 1, 2, \ldots, 5$. This eigenvalue relation (Eq. (2.5)) can now provide the remaining five supermodes DS_{l1}. Note that for the form assumed, $\sum_{n=1}^{6} u_n = 0$ which is consistent with the assumption that the DS_{lm} fields are zero at the center ($u_0 = 0$) when l is finite. Fig. 1(b) illustrate the field profile of the DS_{11} supermode.

This same principle can now be applied to other honeycomb lattices having more rings. As a next example we consider a 19-element honeycomb double ring structure as shown in Fig. 2(a). Given the topology of this configuration, the elements involved are now classified in four groups denoted as a, b, c, and$d$—illustrated with different colors. As in the previous section,

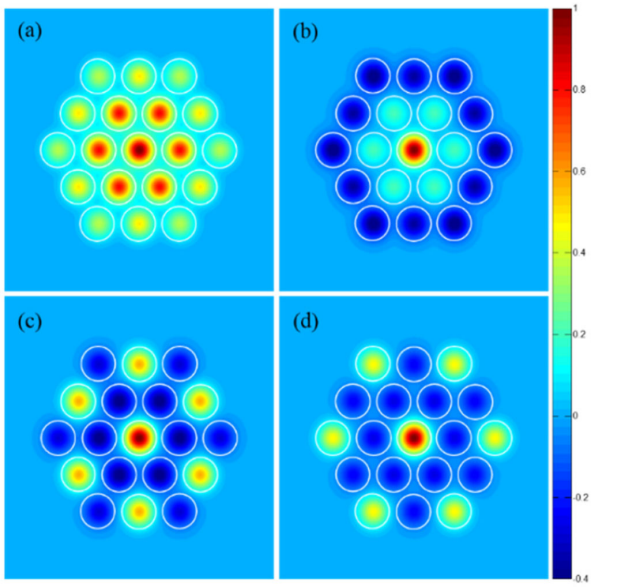

Fig. 3. Real part of the modal field distributions in a 19-core lattice, associated with (a) the DS_{01} (b)DS_{02} (c) DS_{03} (d) DS_{04} supermodes.

because of the hexagonal geometry, all waveguides interact only with their nearest neighbors with a coupling strength κ. Higher order interactions are here ignored since the coupling coefficient tends to exponentially decrease with distance. We now look for in-phase supermodes with $l = 0$. In this situation, the corresponding evolution equations for the modal fields, for these four groups, read as follows:

$$i\frac{d}{dZ}\begin{bmatrix} u_a \\ u_b \\ u_c \\ u_d \end{bmatrix} + \begin{bmatrix} 0 & 6 & 0 & 0 \\ 1 & 2 & 1 & 2 \\ 0 & 1 & 0 & 2 \\ 0 & 2 & 2 & 0 \end{bmatrix} \begin{bmatrix} u_a \\ u_b \\ u_c \\ u_d \end{bmatrix} = 0. \tag{2.6}$$

Again, the in-phase eigenvalue problem can be obtained using the eigenvectors $u_{a,b,c,d} = u^0_{a,b,c,d} e^{i\lambda Z}$ from where we find that $\lambda^4 - 15\lambda^2 - 2\lambda^3 + 24 = 0$. The four roots of this algebraic equation are given by [$\lambda_1 = 4.8715$, $\lambda_2 = 1.2267$, $\lambda_3 = -1.6215$, $\lambda_4 = -2.4767$] and correspond to the DS_{01}, DS_{02}, DS_{03} and DS_{04} in-phase supermodes. Having found the eigenvalues, the corresponding eigenvectors u^0_a, u^0_b, u^0_c, u^0_d can be evaluated from the matrix of Eq. (2.6). Fig. 3 depicts the real part of modal field profile of the DS_{0m} supermodes. The remaining 15 modes are only possible if the angular momentum l is finite. In this case again the field in the central element is zero ($u_a = 0$). In view of the b, c, and d groups assigned, Fig. 2(b) suggests that

$$i\dot{u}_{b_n} + u_{b_{n+1}} + u_{b_{n-1}} + u_{c_n} + u_{d_n} + u_{d_{n-1}} = 0 \tag{2.7a}$$

$$i\dot{u}_{c_n} + u_{b_n} + u_{d_n} + u_{d_{n-1}} = 0 \tag{2.7b}$$

$$i\dot{u}_{d_n} + u_{b_n} + u_{b_{n+1}} + u_{c_n} + u_{c_{n+1}} = 0 \tag{2.7c}$$

where $\dot{u}_{b_n} = du_{b_n}/dZ$, etc. By employing the ansatz $[u_{b_n}, u_{c_n}, u_{d_n}] = [u^0_{b_n}, u^0_{c_n}, u^0_{d_n}] e^{iQn} e^{i\lambda Z}$ in equation (2.7), we arrive at $\lambda^3 - 2\lambda^2 \cos(Q) - \lambda[4\cos(Q) + 5] - 4\sin^2(Q) = 0$. Again, periodicity demands that $Q = l\pi/3$ where l is $1, 2, \ldots, 5$. The three eigenvalues obtained from this cubic equation are tabulated in Table I for each angular momentum l. In this way the remaining 15 supermodes can be generated through the corresponding eigenvectors of the matrix of Eq. (2.7). As an example, the real part of field profiles of modes DS_{11}, DS_{21} and DS_{31} are shown in Fig. 4(a), (b), and (c).

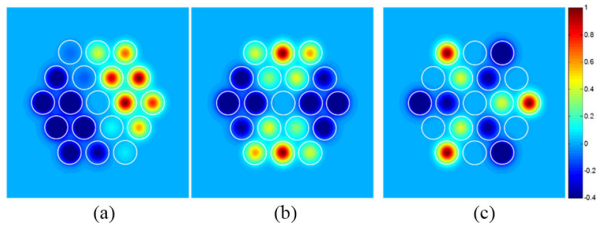

Fig. 4. Real part of the modal field distributions in a 19-core lattice, associated with supermodes having angular momenta (a) DS_{11} (b) DS_{21} and (c) DS_{31} mode.

TABLE I
THE LIST OF EIGENVALUES OBTAINED FROM THE CUBIC EQUATION FOR THE MODES WITH ANGULAR MOMENTUM

Q	Eigenvalues
1	$\lambda = 3.354, -0.476, -1.877$
2	$\lambda = \sqrt{3}, 1, -\sqrt{3}$
3	$\lambda = -1 + \sqrt{2}, 0, -1 - \sqrt{2}$
4	$\lambda = \sqrt{3}, 1, -\sqrt{3}$
5	$\lambda = 3.354, -0.476, -1.877$

Other variations of these hexagonal lattices can also be investigated using this method. For example let us consider again the 19-site configuration when this time the central waveguide is now completely removed. Using the same grouping outlined above, the in-phase modes satisfy

$$i\frac{d}{dZ}\begin{bmatrix} u_b \\ u_c \\ u_d \end{bmatrix} + \begin{bmatrix} 2 & 1 & 2 \\ 1 & 0 & 2 \\ 2 & 2 & 0 \end{bmatrix} \begin{bmatrix} u_b \\ u_c \\ u_d \end{bmatrix} = 0 \tag{2.8}$$

and hence the eigenvalue equation is given by $\lambda^3 - 2\lambda^2 - 9\lambda = 0$, having three roots $\lambda = -2.1623, 0, 4.1623$. One can show that the remaining 15 modes (DS_{lm}) of this 18-site arrangement are identical to those obtained for the 19-site lattice when $l = 1, 2, \ldots, 5$.

As a final example, we investigate a 37 (three layer) hexagonal lattice consisting of single-mode waveguides as shown in Fig. 5(a). Because of their topology, the elements are now grouped in seven families (a, b, c, d, e, f, and g) as illustrated with different colors in Fig. 5(a). Assuming in-phase modes, we find

$$i\frac{d}{dZ}\begin{bmatrix} u_a \\ u_b \\ u_c \\ u_d \\ u_e \\ u_f \\ u_g \end{bmatrix} + \begin{bmatrix} 0 & 6 & 0 & 0 & 0 & 0 & 0 \\ 1 & 2 & 1 & 2 & 0 & 0 & 0 \\ 0 & 1 & 0 & 2 & 1 & 1 & 1 \\ 0 & 2 & 2 & 0 & 0 & 1 & 1 \\ 0 & 0 & 1 & 0 & 0 & 1 & 1 \\ 0 & 0 & 1 & 1 & 1 & 0 & 1 \\ 0 & 0 & 1 & 1 & 1 & 1 & 0 \end{bmatrix} \begin{bmatrix} u_a \\ u_b \\ u_c \\ u_d \\ u_e \\ u_f \\ u_g \end{bmatrix} = 0. \tag{2.9}$$

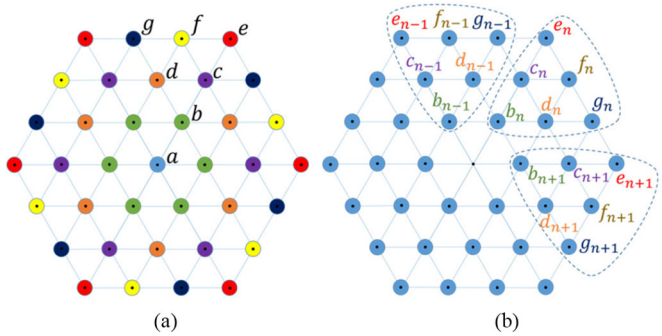

Fig. 5. (a) 37-core hexagonal lattice. The waveguide elements are now grouped in seven different families (a, b, c, d, e, f, g) indicated with different colors. (b) By excluding the central core, the remaining elements of these families are grouped in each hexagonal sector in order to obtain all the supermodes with angular momenta.

Seven supermodes DS_{0m} can then be obtained from the resulting algebraic eigenvalue equation $\lambda^7 - 2\lambda^6 - 23\lambda^5 - 2\lambda^4 + 124\lambda^3 + 164\lambda^2 + 46\lambda - 12 = 0$. The seven roots of this latter equation are given by $\lambda = 5.3492, 2.9752, 0.1594, -0.9524, -1.0000, -1.8567, -2.6748$. As before, the remaining 30 supermodes exhibit angular momentum. These can be determined from the field evolution equations

$$i\dot{u}_{b_n} + u_{b_{n+1}} + u_{b_{n-1}} + u_{c_n} + u_{d_n} + u_{d_{n-1}} = 0 \quad (2.10a)$$

$$i\dot{u}_{c_n} + u_{b_n} + u_{d_n} + u_{d_{n-1}} + u_{e_n} + u_{f_n} + u_{g_{n-1}} = 0 \quad (2.10b)$$

$$i\dot{u}_{d_n} + u_{b_n} + u_{b_{n+1}} + u_{c_n} + u_{c_{n+1}} + u_{f_n} + u_{g_n} = 0 \quad (2.10c)$$

$$i\dot{u}_{e_n} + u_{c_n} + u_{f_n} + u_{g_{n-1}} = 0 \quad (2.10d)$$

$$i\dot{u}_{f_n} + u_{c_n} + u_{d_n} + u_{e_n} + u_{g_n} = 0 \quad (2.10e)$$

$$i\dot{u}_{g_n} + u_{c_{n+1}} + u_{d_n} + u_{f_n} + u_{e_{n+1}} = 0. \quad (2.10f)$$

By employing the ansatz $u_{x_n} = u^0_{x_n} e^{i\lambda Z} e^{iQn}$ we find

$$\lambda^6 - 2\lambda^5 \cos(Q) - \lambda^4 (4\cos(Q) + 13) + \lambda^3 \left(4\cos^2(Q) + 8\cos(Q) - 14\right) + \lambda^2 \left(16\cos^2(Q) + 18\cos(Q) + 18\right) + \lambda \left(6\cos(2Q) + 20\cos^2(Q) + 8\cos(Q) + 22\right) + \left(8\cos(2Q) + 8\cos^2(Q) + 4\cos(Q) - 4\cos(2Q)\cos(Q)\right) = 0 \quad (2.11)$$

where $Q = l\pi/3$ with $l = 1, 2, \ldots, 5$. The 6×5 eigenvalues of these DS_{lm} supermodes (carrying angular momentum) can be directly obtained from Eq. (2.11) along with their eigenvectors. The real part of modal field profiles of the DS_{03}, DS_{04}, DS_{21}, DS_{23}, DS_{32} and DS_{35} is depicted in Fig. 6. Finally the eigenvalue distributions and degeneracies of a 7-, 19-, 37-core lattice are provided for comparison in Fig. 7. We would like to note that in all cases our results (based on coupled-mode theory) are in excellent agreement with finite element simulations

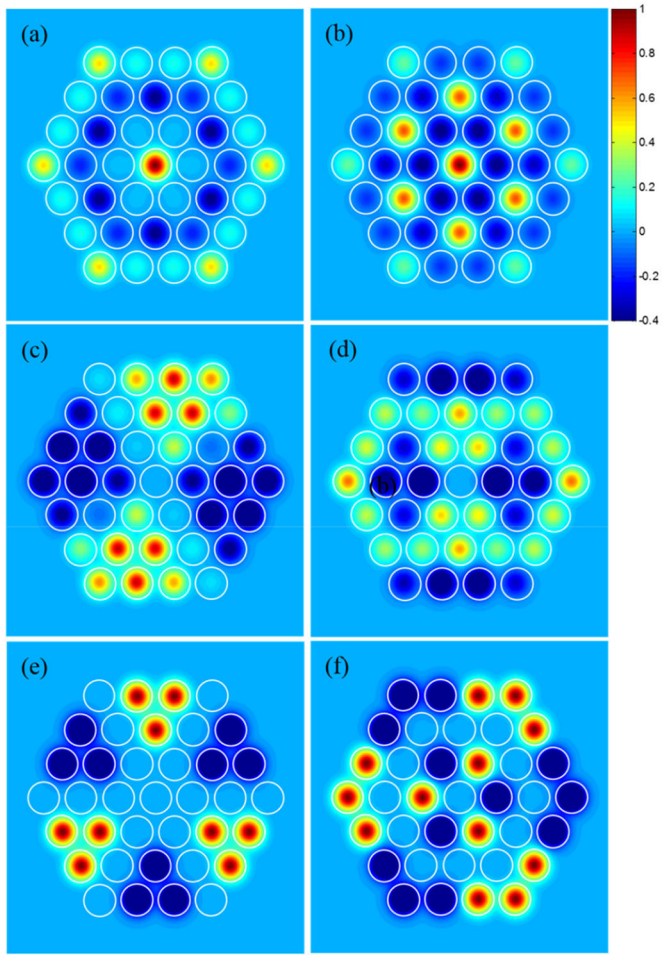

Fig. 6. Real part of the modal field distributions in a 37-core lattice, associated with supermodes (a) DS_{03} (b) DS_{04} (c) DS_{21} (d) DS_{23} (e) DS_{32} (f) DS_{35}.

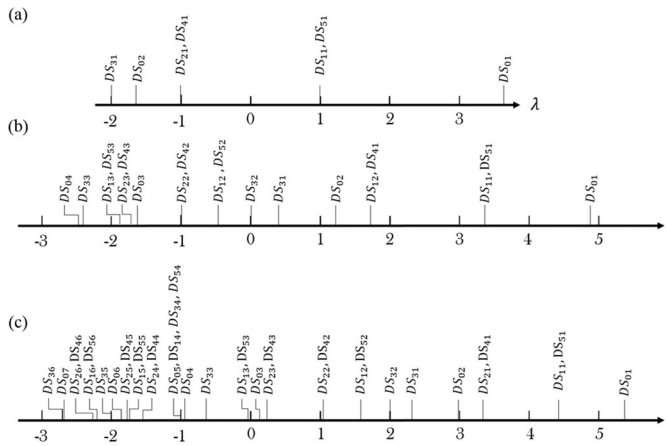

Fig. 7. Eigenvalue distribution diagrams for (a) a 7-core (b) 19-core and (c) 37-core hexagonal lattice.

based on weakly guiding structures. The method described here can be used in a similar fashion to analyze any other multi-ring hexagonal lattice. For example, in the case of a 61-core hexagonal lattice (involving four layers), the grouping of the elements will lead to 11 in-phase DS_{0m} supermodes (whose eigenvalues are obtained from a 11th order polynomial) while 10×5 DS_{lm}

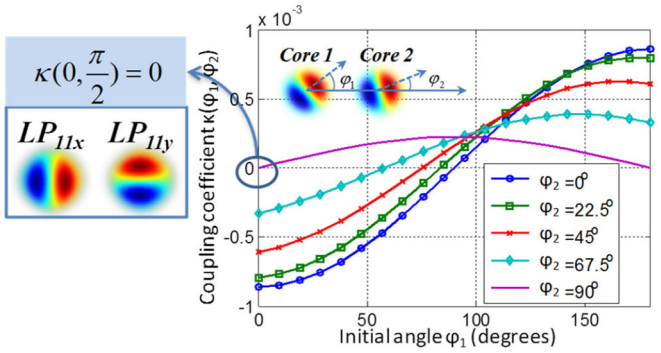

Fig. 8. Coupling between two arbitrarily oriented LP_{11} degenerate modes as a function of their initial angles φ_1 and φ_2. The arrow points to the position of zero coupling $\kappa(\varphi_1 = 0, \varphi_2 = \pi/2) = 0$ between the LP_{11x} and LP_{11y} modes; the inset shows the coordinate system of the two cores including reference axes and two initial angles.

supermodes with angular momentum can result from a 10th order polynomial involving $Q = l\pi/3$where $l = 1, 2, \ldots, 5$.

III. Theory of Higher-Order Supermodes

When the guiding power is increased for an isolated core, it can guide high-order modes. For optical fibers with low refractive index contrast, the vector modes are weakly guided and therefore can be treated as linear polarization (LP) modes. In essence, the LP modes are scalar approximations of the vector mode fields and contain only one transverse field component given by,

$$E_{pq}(r,\theta) = \begin{cases} U\dfrac{J_p(\kappa_{pq}\cdot r)}{J_p(\kappa_{pq}\cdot a)}\cos(p\theta+\varphi), \text{for} r \le a \\ U\dfrac{K_p(\gamma_{pq}\cdot r)}{K_p(\gamma_{pq}\cdot a)}\cos(p\theta+\varphi), \text{for} r > a \end{cases} \tag{3.1}$$

where U is the complex amplitude, J and K are Bessel functions of the first and second kind, a is the core radius, φ is an arbitrary start angle, and p is a non-negative integer referred to as the azimuthal mode order. For the same p value, κ_{pq} and γ_{pq} can take on multiple discrete values determined from the dispersion relation. Therefore it is appropriate to label each of the aforementioned terms with another non-negative integer corresponding to the number of times the field crosses zero along the radial direction. Thus, the LP modes can be labeled as LP_{pq}. The orthogonal field component is the same as Eq. (3.1) therefore the results presented here applies to either polarization. According to Eq. (3.1), when $p > 0$, the modal field has an additional degree of freedom in the azimuthal direction because the start angle φ is arbitrary, which generates spatially orthogonal modes even if both p and q are the same. For example the LP_{11x} and LP_{11y} modes correspond to the cases of $\varphi = 0$ and $\varphi = \pi/2$, respectively, shown in Fig. 8. This is very different from the case of $p = 0$ where the LP_{0q} modal field is azimuthally uniform and has no spatial degeneracy.

To the best of our knowledge, until now the study of supermodes has been limited to the supermodes composed of these azimuthally uniform $LP_{pq}(p = 0)$ "core modes," particularly LP_{01} supermodes. However, the higher-order LP_{pq} $(p > 0)$ "core modes" can also form supermodes. Moreover, these supermodes are strongly affected by the geometrical distribution of the cores within the MCF, because the coupling of LP_{pq} $(p > 0)$ modes between two cores varies significantly with initial angles of the modes. We name these angle-dependent supermodes as "higher-order supermodes." Unlike the higher-order core modes (p or $p < 0$), higher-order supermodes specifically refer to the supermodes formed because of coupling among "core modes" with $p > 0$. In this section, we begin the study of higher-order supermodes from the simplest two-core structure by demonstrating how angle-dependent coupling influences the eigenmode formation. Then, we extend the theory to more complex geometrical structures, using symmetries to produce analytical formulas for higher-order supermodes. More specifically, we derive formulas for commonly used formations, including linear-array, grid-array and ring-array structures.

A. Higher-Order Supermodes in a Two-Core Structure

As described above, the coupling between two LP_{pq} $(p > 0)$ modes strongly depends on the initial angles of both modes. In order to focus on this angular dependence, the LP_{pq} $(p > 0)$ modal field of Eq. (3.1) is written as a function of the initial angle φ

$$\begin{aligned} E(\varphi) &= F_r \cdot \cos(p\theta - \varphi) \\ &= E_x \cdot \cos\varphi + E_y \cdot \sin\varphi \end{aligned} \tag{3.2}$$

where F_r represents the radial component of the modal field, $E_x = E(\varphi = 0)$ and $E_y = E(\varphi = \frac{\pi}{2})$ correspond to the modal fields aligned with the horizontal axis x and vertical axis y. A coordinate system is selected where the azimuthal reference axis is parallel to the edge of the graph formed by vertices at the center of the isolated cores as shown in the inset of Fig. 8. The coupling coefficient between two LP_{pq} $(p > 0)$ modal fields with initial angles of φ_1 and φ_2, respectively, in the two identical cores 1 and 2 is given by

$$\begin{aligned} \kappa(E_1(\varphi_1), E_2(\varphi_2)) = {} & \frac{\omega}{2}\iint_{\text{core2}} \varepsilon_0(n_{CoreB}^2 - n_{Clad}^2) \\ & \cdot E_1^*(\varphi_1)\cdot E_2(\varphi_2)dxdy \\ = {} & \kappa_x \cdot \cos\varphi_1\cos\varphi_2 + \kappa_y \\ & \cdot \sin\varphi_1\sin\varphi_2 + \cdots \kappa_{xy} \\ & \cdot \cos\varphi_1\sin\varphi_2 + \kappa_{yx}\cdot\sin\varphi_1\cos\varphi_2 \end{aligned} \tag{3.3}$$

where $\kappa_x = \kappa(E_{1,x}, E_{2,x})$, $\kappa_y = \kappa(E_{1,y}, E_{2,y})$, $\kappa_{xy} = \kappa(E_{1,x}, E_{2,y})$, $\kappa_{yx} = \kappa(E_{1,y}, E_{2,x})$. The modal fields are normalized, ε_0 and ω are vacuum permittivity and angular frequency, n_{Core2} and n_{Clad} are the refractive indices of core 2 and the cladding, respectively. Fig. 8 represents the typical behavior of the coupling coefficient as the initial angles of two LP_{11} modes change, according to Eq. (3.3). $\kappa_x > \kappa_y > 0$ is observed as a result of the specific geometrical distribution of modal fields with respect to the cores. More importantly, coupling vanished for two specific initial angles,

i.e., $\kappa_{xy} = \kappa_{yx} = 0$, as illustrated in by the arrow in Fig. 8. This phenomenon occurs because the mirror-reversal of two modal fields across an axis parallel to the reference axis should have the same coupling coefficient, which can be mathematically elaborated as

$$\begin{aligned}\kappa_{xy} &= \frac{\omega}{2}\iint_{\text{core2}} \varepsilon_0(n^2_{\text{Core}B} - n^2_{\text{Clad}}) \\ &\quad \cdot F^*_{1,r}\cos(\theta_1)\cdot F_{2,r}\sin(\theta_2)dxdy \\ &= \frac{\omega}{2}\iint_{\text{Core2}} \varepsilon_0(n^2_{\text{Core}B} - n^2_{\text{Clad}}) \\ &\quad \cdot F^*_{1,r}\cos(-\theta_1)\cdot F_{2,r}\sin(-\theta_2)dxdy \\ &= -\kappa_{yx} = 0. \end{aligned} \tag{3.4}$$

With this result, Eq. (3.3) can be immediately simplified as

$$\begin{aligned}\kappa(E_1(\varphi_1), E_2(\varphi_2)) = \ & \kappa_\chi \cdot \cos\varphi_1 \cos\varphi_2 \\ & + \kappa_y \cdot \sin\varphi_1 \sin\varphi_2. \end{aligned} \tag{3.5}$$

Similar to the LP_{01} supermodes, higher-order supermodes can be investigated using coupled-mode theory under the assumption of weak coupling. For the simplest case of the two-core structure, the basis set for each core is strategically chosen as the E_x and E_y pair, even though it could have been any orthogonal set with an arbitrary initial angle. Then the interactions between the "core modes" can be described by the following coupled-mode equation in a matrix form

$$i\frac{d}{dz}\boldsymbol{U} + \bar{\boldsymbol{M}}\boldsymbol{U} = 0, \tag{3.6}$$

where $\boldsymbol{U} = [\,u_{1,x}\ u_{2,x}\ u_{1,y}\ u_{2,y}\,]^T$; $u_{m,x}$ or $u_{m,y}$ are the complex amplitude of the horizontally or vertically aligned modal field of the mth core after adopting the gauge transformation $u_{m,x/y} = U_{m,x/y}\cdot e^{i\beta_0 z}$ in which β_0 is the propagation constant of any isolated core mode LP_{pq}; and hence $\bar{\boldsymbol{M}}$ is a 4×4 coupled matrix

$$\bar{\boldsymbol{M}} = \begin{bmatrix} 0 & \kappa_x & 0 & \kappa_{xy} \\ \kappa_x & 0 & \kappa_{xy} & 0 \\ 0 & \kappa_{yx} & 0 & \kappa_y \\ \kappa_{yx} & 0 & \kappa_y & 0 \end{bmatrix}. \tag{3.7}$$

The standard procedure of solving the coupled-mode equation is to diagonalize the coupled matrix $\boldsymbol{Q}^{-1}\bar{\boldsymbol{M}}\boldsymbol{Q} = \boldsymbol{\Lambda}$ where the eigenvalues λ give the normalized propagation constants of the supermodes. The corresponding eigenvectors $\boldsymbol{U}' = \boldsymbol{Q}^{-1}\boldsymbol{U}$ describes the supermode field amplitudes and the row vectors of $\boldsymbol{A} = \boldsymbol{Q}^{-1}$ represents the amplitude coefficients of superposition of core modes in forming the supermodes. In the supermode basis, the coupled-mode equation reduces to

$$i\frac{d}{dz}\boldsymbol{U}' + \boldsymbol{\Lambda}U' = 0. \tag{3.8}$$

For this particular coupled-mode equation, one can apply $\kappa_{xy} = \kappa_{yx} = 0$ first and then divide the equation into two

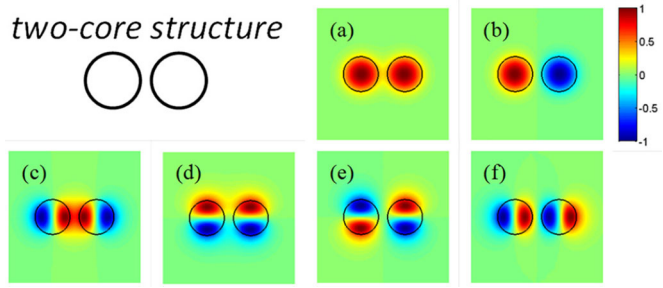

Fig. 9. Modal fields of LP_{01} supermodes (a and b) and LP_{11} supermodes (c)–(f) of a basic two-core structure. In-phase supermodes are shown in (a), (c) and (d) while out-of phase supermodes are shown in (b), (e) and (f).

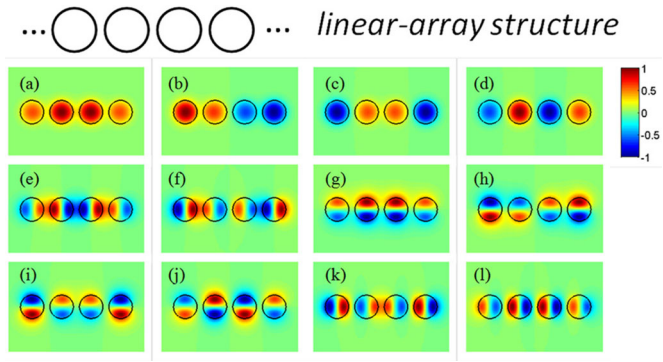

Fig. 10. Modal fields of LP_{01} supermodes (a)–(d) and LP_{11} supermodes (e)–(l) of a 4-core linear-array structure.

reduced ones as follows:

$$i\frac{d}{dz}\begin{bmatrix} u_{1,x} \\ u_{2,x} \end{bmatrix} + \begin{bmatrix} 0 & \kappa_x \\ \kappa_x & 0 \end{bmatrix}\begin{bmatrix} u_{1,x} \\ u_{2,x} \end{bmatrix} = 0 \tag{3.9a}$$

$$i\frac{d}{dz}\begin{bmatrix} u_{1,y} \\ u_{2,y} \end{bmatrix} + \begin{bmatrix} 0 & \kappa_y \\ \kappa_y & 0 \end{bmatrix}\begin{bmatrix} u_{1,y} \\ u_{2,y} \end{bmatrix} = 0. \tag{3.9b}$$

The above equations mean that E_x and E_y, the horizontally and vertically aligned "core modes" do not "talk to" each other and their formation of higher-order supermodes can be solved separately. Eqs. (3.9a) and (3.9b) turn out to be very similar to those for the case of LP_{01} supermodes. The amplitude coefficients of the higher-order supermode corresponding to the row vectors of $\boldsymbol{A} = \boldsymbol{Q}^{-1} = \frac{1}{\sqrt{2}}[1, 1; 1, -1]$ are the same as those for the LP_{01} supermodes. For higher-order supermodes composed of E_x and E_y respectively, as shown in Fig. 9, the propagation constants of the four higher-order supermodes $\beta = \beta_0 + \lambda$ are calculated to be $\beta_0 \pm 2\kappa_x$ and $\beta_0 \pm 2\kappa_y$, respectively.

B. Higher-Order Supermodes in Linear-Array Structures with Translational Symmetry

A slightly more complex structure is the linear array where the cores are linearly aligned with each other with equal core-to-core distances as shown in Fig. 10. In this case, couplings between non-adjacent cores are expected to be negligible. Let us start with the LP_{01} supermodes, which do not have angular

dependence. One could solve the eigen-problem of the coupled-mode equation as described in the last section and obtain the supermodes. The alternative method is to find the solutions that satisfy the boundary conditions $u_0 = u_{N+1} = 0$ [24]. As a result, the amplitude of the mth core within any LP_{01} supermode can be described as

$$A_m = a \cdot e^{imQ} + b \cdot e^{-imQ}, m = 1, 2, \cdots N \tag{3.10}$$

where a and b are coefficients; Q is the common phase acquired by shifting any one lattice due to the translational symmetry. The boundary conditions applied to both sides of the linear structure ($m = 0$ and $m = N + 1$)

$$\begin{aligned} A_{N+1} &= a \cdot e^{i(N+1)Q} + b \cdot e^{-i(N+1)Q} \\ &= A_0 = a \cdot e^{i0} + b \cdot e^{-i0} = 0, \end{aligned} \tag{3.11}$$

yield $a + b = 0$ and $Q = \frac{\pi l}{N+1}, l = 1, 2, \ldots N$. Therefore the LP_{01} supermode can be written as

$$u'_{l,m} = A_{l,m} \cdot u_{l,m} = \sin\left(\frac{\pi l m}{N+1}\right) \cdot u_{l,m}, m, l = 1, 2, \cdots N \tag{3.12}$$

where l corresponds to the order of different supermodes and u_m represents the complex amplitude of the mth "core mode." For the lth LP_{01} supermode, comparing the coupled-mode equation

$$i\frac{d}{dz}u_m + \kappa(u_{m-1} + u_{m+1}) = 0, \tag{3.13}$$

with the supermode equation

$$i\frac{d}{dz}u'_m + \lambda_l u'_m = 0 \tag{3.14}$$

where κ is the coupling coefficient between two adjacent LP_{01} "core modes," the propagation constant of the lth LP_{01} supermode $\beta_l = \beta_0 + \lambda_l$ can be obtained as

$$\beta_l = \beta_0 + 2\kappa \cdot \cos\left(\frac{\pi l}{N+1}\right), l = 1, 2 \cdots N. \tag{3.15}$$

For higher-order supermodes, because only coupling between adjacent cores is considered, E_x modes would only couple to themselves as would E_y modes, according to $\kappa_{xy} = \kappa_{yx} = 0$. Therefore the higher-order supermodes of the linear-array structure can be divided into the E_x- and E_y-families; each of them can be solved independently using the same relations as used for the LP_{01} supermode. The propagation constants are attained as

$$\beta_{l,x} = \beta_0 + 2\kappa_x \cdot \cos\left(\frac{\pi l}{N+1}\right), l = 1, 2 \cdots N \tag{3.16a}$$

$$\beta_{l,y} = \beta_0 + 2\kappa_y \cdot \cos\left(\frac{\pi l}{N+1}\right), l = 1, 2 \cdots N \tag{3.16b}$$

respectively. An example of the LP_{11} supermodes as well as the LP_{01} supermodes of a 4-core linear-array structure is shown in Fig. 10.

C. Higher-Order Supermodes in 2D Rectangular-Array Structures with Direct and Diagonal Coupling Interactions

We then analyze the supermodes in two dimensional (2D) discrete waveguide arrays. These are composed of $M \times N$ identical optical waveguides arranged in a rectangular geometry. The distance between cores is taken here to be D. For generality, we also include in our analysis not only nearest neighbor interactions κ (occurring along the horizontal and vertical directions) but also higher-order couplings κ_c taking place along the two diagonals as shown in Fig. 11(a). For weakly guiding structures, the coupling strengths can be obtained from the Eq. (2.1). We first consider supermodes derived from the LP_{01} mode supported by each waveguide channel in a square lattice (see Fig. 11(a)). In such an arrangement, the modal fields evolve according to [26]:

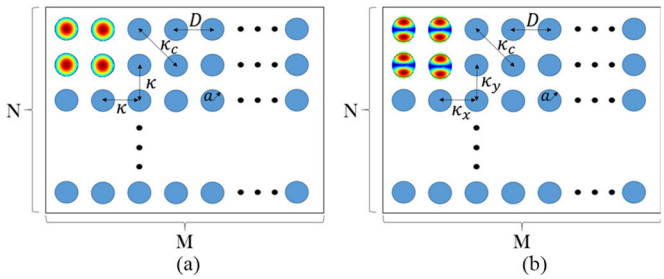

Fig. 11. (a) A rectangular array of waveguides. The LP_{01} mode in each waveguide cross-talks with nearest neighbors along the horizontal and vertical directions as well as with diagonal elements. (b) Coupling interactions in this same array when each element involves instead the LP_{11} mode.

$$\begin{aligned} &i\frac{dU_{m,n}}{dz} + \beta_0 U_{m,n} + \kappa\left(U_{m+1,n} + U_{m-1,n}\right. \\ &\left. + U_{m,n+1} + U_{m,n-1}\right) + \kappa_c\left(U_{m+1,n+1} + U_{m+1,n-1}\right. \\ &\left. + U_{m-1,n+1} + U_{m-1,n-1}\right) = 0 \end{aligned} \tag{3.17}$$

where $U_{n,m}$ represents the modal field amplitude at site n, m in this rectangular array and the discrete site indices take values from the sets $n = 1, 2, \ldots, N$ and $m = 1, 2, \ldots, M$. To identify the eigenmodes of this system, we look for solutions of the type $U_{m,n} = e^{i\beta_0 z}u_{m,n}$ that also satisfy the boundary conditions $u_{m,0} = u_{m,N+1} = u_{0,n} = u_{M+1,n} = 0$ [27]. Based on these requirements, one can directly show that the $U^{k,l}$ supermodes of this structure are $U^{k,l}_{m,n} = A^{k,l}_{m,n}e^{i\beta_0 z}e^{i\lambda_{k,l}z}$ with the amplitudes given by

$$A^{k,l}_{m,n} = \sin\left(m\frac{k\pi}{M+1}\right)\sin\left(n\frac{l\pi}{N+1}\right) \tag{3.18}$$

where $k = 1, 2, \ldots, M$ and $l = 1, \ldots, N$. In addition, the eigenvalue associated with $U^{k,l}$ supermode is given by

$$\begin{aligned} \lambda_{k,l} = {} & 2\kappa\left[\cos\left(\frac{k\pi}{M+1}\right) + \cos\left(\frac{l\pi}{N+1}\right)\right] + \\ & 4\kappa_c \cos\left(\frac{k\pi}{M+1}\right)\cos\left(\frac{l\pi}{N+1}\right). \end{aligned} \tag{3.19}$$

Evidently, altogether this array supports $M \times N$ supermodes. Similarly, one can investigate the eigenmodes of this same array arising from the LP_{11} mode of each waveguide (see Fig. 11(b)). In a weakly coupled array, the LP_{11} mode tends to orient itself either along the x or y direction (LP_{11x}, LP_{11y}). As a result the coupling strengths κ_x and κ_y are different because of

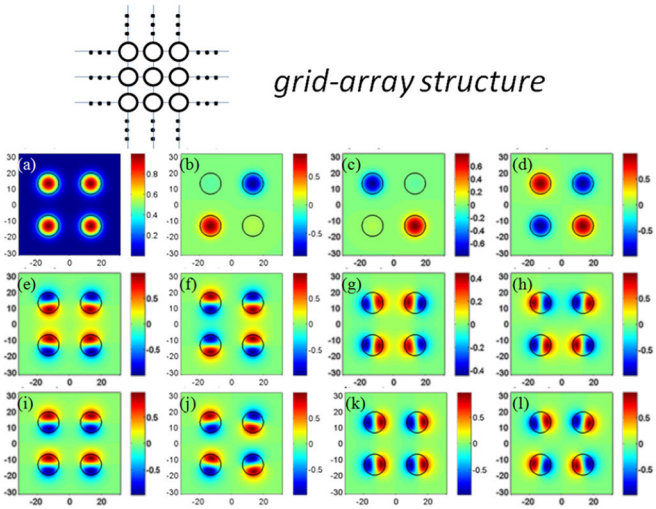

Fig. 12. (a) Scheme of mode basis selection for LP_{11} supermode analysis of a 4-core grid-array structure; modal fields of LP_{01} supermodes (a)–(d) and LP_{11} supermodes (e)–(l) of a 4-core grid-array structure computed using COMSOL.

their respective overlap integrals. Hence, the field evolution is described by

$$i\frac{dU_{m,n}}{dz} + \beta_0 U_{m,n} + \kappa_x \left(U_{m+1,n} + U_{m-1,n}\right) + \kappa_y \left(U_{m,n+1} + U_{m,n-1}\right) + \kappa_c \left(U_{m+1,n+1} + U_{m+1,n-1} + U_{m-1,n+1} + U_{m-1,n-1}\right) = 0. \tag{3.20}$$

The supermodes $U^{k,l}$ of this latter equation are exactly identical in form with those provided by Eq. (3.18). In this case however, the corresponding eigenvalues are given by

$$\lambda_{k,l} = 2\kappa_x \cos\left(\frac{k\pi}{M+1}\right) + 2\kappa_y \cos\left(\frac{l\pi}{N+1}\right) + 4\kappa_c \cos\left(\frac{k\pi}{M+1}\right)\cos\left(\frac{l\pi}{N+1}\right). \tag{3.21}$$

In all cases our results (based on coupled-mode theory) are in excellent agreement with finite element simulations using COMSOL as shown in Fig. 12.

D. Higher-Order Supermodes in Ring-Array Structures with Rotational Symmetry

Ring-array structure is another interesting geometry for higher-order supermodes as it possesses rotational symmetry. Here also, we only consider coupling between adjacent cores. We start from LP_{01} supermodes of N-core ring-array structure. In this case, the coupled matrix $\bar{\boldsymbol{M}}$ is a symmetric circulant matrix. If β_0 and κ are defined as the propagation constant of the "core mode" and the coupling coefficient between two adjacent LP_{01} "core modes" respectively, the elements of the N × N coupled matrix are given as

$$(\bar{\boldsymbol{M}})_{lm} = \beta_0 \delta_{lm} + \kappa\left(\delta_{l+1,m} + \delta_{l,m+1}\right) \tag{3.22}$$

where δ_{lm}, $\delta_{l+1,m}$ and $\delta_{l,m+1}$ are Kronecker deltas; l and m are integer numbers mod N. This matrix can be diagonalized by a lattice Fourier transform as $\boldsymbol{\Lambda} = \boldsymbol{Q}^{-1}\bar{\boldsymbol{M}}\boldsymbol{Q}$ [5]. $\boldsymbol{Q}^{-1}$ is a unitary matrix with elements given as

$$(\boldsymbol{Q}^{-1})_{lm} = \frac{1}{\sqrt{N}} e^{i\frac{2\pi l}{N}\cdot m} \tag{3.23}$$

which represents the amplitude of mth core for the lth LP_{01} supermode. These discrete helical phases give supermodes an appearance similar to optical vortices but in a discrete form and thus carry orbital angular momentum [4]. The propagation constant of the lth LP_{01} supermode equals the corresponding eigenvalue and can be calculated as

$$\beta_l = \beta_0 + 2\kappa \cdot \cos\left(\frac{2\pi l}{N}\right), l = 1, 2 \cdots N. \tag{3.24}$$

According to Eq. (3.24), it is obvious that the lth and $(N-l)$th supermodes are degenerate modes. This has a physical explanation from the equivalence between clockwise and counter-clockwise mode orders. A unitary transformation can project the vortex-like basis of the lth and $(N-l)$th supermodes into another orthogonal basis. In particular, the degenerate supermodes can be transformed into a basis in real fields with amplitude transformation as below

$$\begin{bmatrix} B_{l,m} \\ B_{N-l,m} \end{bmatrix} = \frac{1}{\sqrt{2}} \begin{bmatrix} 1 & 1 \\ 1 & -1 \end{bmatrix} \begin{bmatrix} A_{l,m} \\ A_{N-l,m} \end{bmatrix} \tag{3.25}$$

where $B_{l,m} = \sqrt{\frac{2}{N}} \cos\left(\frac{2\pi l}{N} \cdot m\right)$ and $B_{N-l,m} = \sqrt{\frac{2}{N}} \sin\left(\frac{2\pi l}{N} \cdot m\right)$.

The higher-order supermodes of ring-array structure are particularly interesting because they can no longer be divided into E_x- and E_y-basis for independent analysis. Instead, the tangential and normal mode basis E_{t_m} and E_{n_m} (m refers to the core number) are selected, which correspond to "core modes" aligned horizontally or vertically with respect to the reference axis pointing from the ring center to the mth core. Fig. 13(a) shows such a mode basis for a 3-core ring-array structure. In that case, $\kappa_{1,2} = \kappa_{2,3} = \kappa_{3,1}$ is obtained because of the rotational symmetry. In addition, the coupling coefficients between the LP_{pq} modes are real so that $\kappa_{i,j} = \kappa_{j,i}$. Therefore the number of coupling coefficients for the N-core ring-array structure is reduced from 2N to 4 given by

$$\kappa_{t_1,t_2} = -\kappa_x \sin^2\left(\frac{\pi}{N}\right) + \kappa_y \cos^2\left(\frac{\pi}{N}\right), \tag{3.26a}$$

$$\kappa_{t_1,n_2} = -\kappa_x \sin\left(\frac{\pi}{N}\right)\cos\left(\frac{\pi}{N}\right) - \kappa_y \sin\left(\frac{\pi}{N}\right)\cos\left(\frac{\pi}{N}\right), \tag{3.26b}$$

$$\kappa_{n_1,t_2} = \kappa_x \sin\left(\frac{\pi}{N}\right)\cos\left(\frac{\pi}{N}\right) + \kappa_y \sin\left(\frac{\pi}{N}\right)\cos\left(\frac{\pi}{N}\right), \tag{3.26c}$$

$$\kappa_{n_1,n_2} = \kappa_x \cos^2\left(\frac{\pi}{N}\right) - \kappa_y \sin^2\left(\frac{\pi}{N}\right). \tag{3.26d}$$

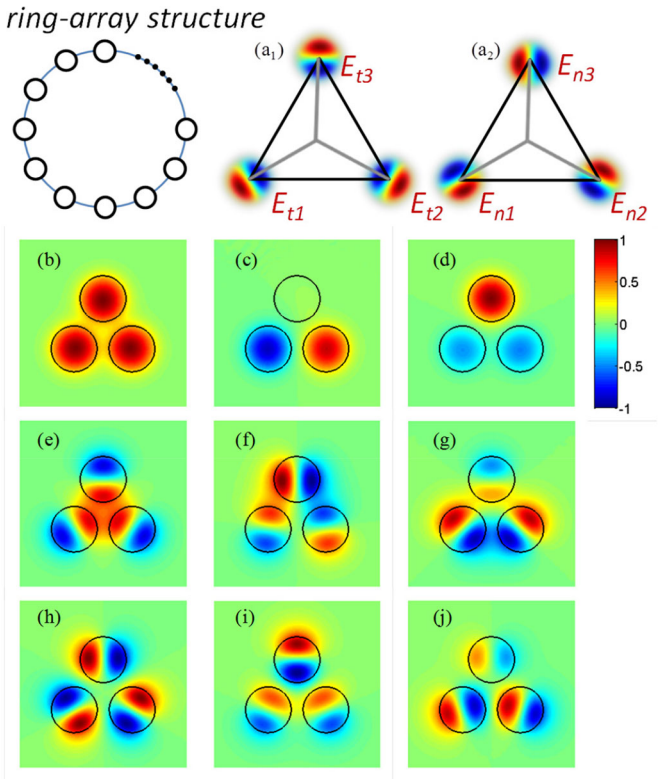

Fig. 13. (a) Scheme of mode basis selection for LP_{11} supermode analysis of a 3-core ring-array structure; modal fields of LP_{01} supermodes (b)–(d) and LP_{11} supermodes (e)–(j) of a 3-core ring-array structure computed using COMSOL.

Then the coupled-mode equation for the N-core ring-array can be written as

$$i\frac{d}{dz}\begin{bmatrix}\boldsymbol{U}_t\\ \boldsymbol{U}_n\end{bmatrix}+\bar{\boldsymbol{M}}\begin{bmatrix}\boldsymbol{U}_t\\ \boldsymbol{U}_n\end{bmatrix}=0, \tag{3.27}$$

where $\boldsymbol{U}_t$ and $\boldsymbol{U}_n$ are column vectors of dimension N. the coupled matrix

$$\bar{\boldsymbol{M}}=\begin{bmatrix}\boldsymbol{M}_{tt} & \boldsymbol{M}_{tn}\\ \boldsymbol{M}_{nt} & \boldsymbol{M}_{nn}\end{bmatrix}$$

is a rank-2N Hermitian matrix and each sub-matrix is a circulant matrix with elements described as

$$(\boldsymbol{M}_{tt})_{lm} = \kappa_{t_1,t_2}\left(\delta_{l+1,m}+\delta_{l,m+1}\right), \tag{3.28a}$$
$$(\boldsymbol{M}_{tn})_{lm} = \kappa_{t_1,n_2}\delta_{l+1,m}+\kappa_{n_1,t_2}\delta_{l,m+1}, \tag{3.28b}$$
$$(\boldsymbol{M}_{nt})_{lm} = \kappa_{n_1,t_2}\delta_{l+1,m}+\kappa_{t_1,n_2}\delta_{l,m+1}, \tag{3.28c}$$
$$(\boldsymbol{M}_{nn})_{lm} = \kappa_{n_1,n_2}\cdot\left(\delta_{l,m+1}+\delta_{l+1,m}\right). \tag{3.28d}$$

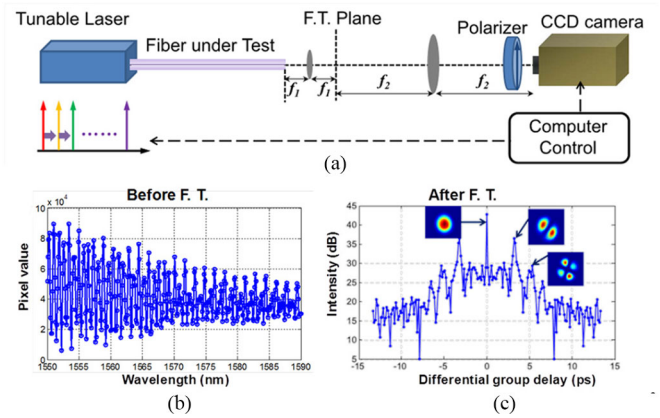

Fig. 14. (a) Schematic of spatially-and-spectrally-resolved imaging (S^2 imaging) setup using a tunable laser and a CCD camera; (b) wavelength-scanning results of the multi-path interference pattern for one pixel of the CCD camera and (c) the result of intensity vs. differential group delay (DGD) after taking Fourier transform of (b) for the same pixel. Inset of (c) shows the resolved LP modes after picking the information for every pixel at the corresponding DGDs of different modes and mapping them together.

where δ_{lm}, $\delta_{l+1,m}$ and $\delta_{l,m+1}$ are the Kronecker deltas; l and m are integer numbers mod N. Diagonalization of the coupled matrix $\boldsymbol{M}$ is the key to solving the higher-order supermodes. It takes two steps as follows as described in appendix A.

Both the eigenvalues and eigenvectors can be obtained after successful diagonalization of the coupled matrix. After plugging the coupling coefficients into the eigenvalues and eigenvectors using Eq. (3.22), the higher-order supermodes can be divided into $(\pm)$ groups and solved as Eq. (3.29), shown at the bottom of the page, where

$$\gamma_l^{(\pm)}=-i\left(\eta\pm\sqrt{1+\eta^2}\right)$$

and

$$\eta=\frac{(\kappa_x-\kappa_y)\cot\left(\frac{2\pi l}{N}\right)}{(\kappa_x+\kappa_y)\sin\left(\frac{2\pi l}{N}\right)}.$$

The propagation constants of the higher-order supermodes are the eigenvalues

$$\beta_l^{(\pm)}=\beta_0+(\kappa_x+\kappa_y)\cdot\cos\left(\frac{2\pi}{N}\right)\cdot\cos\left(\frac{2\pi l}{N}\right)\pm\ldots$$
$$\sqrt{(\kappa_x-\kappa_y)^2\cdot\cos^2\left(\frac{2\pi l}{N}\right)+(\kappa_x+\kappa_y)^2\cdot\sin^2\left(\frac{2\pi}{N}\right)\cdot\sin^2\left(\frac{2\pi l}{N}\right)}, \tag{3.30}$$

where $l=1,2\cdots N$. Same as the LP_{01}supermodes, the lth and $(N-l)$th higher-order supermodes for both $(\pm)$ groups

$$E_l^{(\pm)}=\begin{cases}\sum_{m=1}^{N}\left(e^{i\frac{2\pi l}{N}\cdot m}E_{t_m}\right)+\gamma_l^{(\pm)}\cdot\sum_{m=1}^{N}\left(e^{i\frac{2\pi l}{N}\cdot m}E_{n_m}\right), \text{if } \sin\left(\frac{2\pi l}{N}\right)\neq 0\\ \sum_{m=1}^{N}\left(e^{i\frac{2\pi l}{N}\cdot m}E_{t_m}\right) \text{or } \sum_{m=1}^{N}\left(e^{i\frac{2\pi l}{N}\cdot m}E_{n_m}\right), \text{if } \sin\left(\frac{2\pi l}{N}\right)=0\end{cases} \tag{3.29}$$

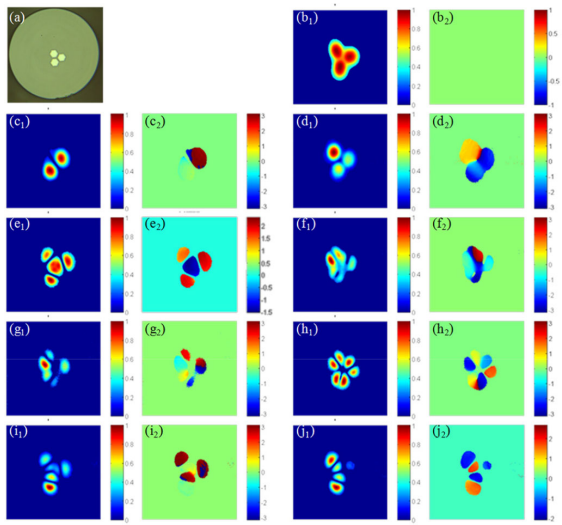

Fig. 15. (a) Cross-sectional view of the fabricated coupled-3-core fiber and (b)–(j) resolved supermodes of the fabricated coupled-3-core fiber shown in amplitude (x_1) and phase (x_2): (b) the fundamental LP_{01} supermode; (c), (d) the degenerate pair of LP_{01} supermodes; (d) the fundamental LP_{11} supermode; (e), (f) the first degenerate pair of LP_{11} supermodes; (g) the fourth LP_{11} supermode; (h), (i) the second degenerate pair of LP_{11} supermodes.

are degenerate. Real-field basis can be obtained by applying a unitary transformation on the current basis. An example of the LP_{11}supermodes as well as the LP_{01}-supermodes of a 3-core ring-array structure is shown in Fig. 13(b)–(j).

IV. Observation of Higher-Order Supermodes

A coupled few-mode 3-core fiber was fabricated in order to observe higher-order supermodes. The cross-section of the fiber is shown in Fig. 15(a), where the Ge-doped cores are hexagonally-shaped as a result of the stack-and-draw fabrication process. The cladding diameter is ∼120 μm, and the index difference between the core and cladding is ∼0.6%. The core diameter was selected to be ∼9 μm to ensure that the cut-off wavelength of the fundamental modes is well above 1.5 μm. In addition, the core pitch was chosen to be ∼11.5 μm, a small enough distance to allow for strong coupling. Therefore the fiber supports both LP_{01} and LP_{11} supermodes around 1.5 μm.

A spectrally-and-spatially resolved imaging (S^2 imaging) setup was built to acquire the modal fields from the fiber. The S^2 imaging procedure, first developed by Nicholson *et al.* [28], is a technique specially designed for quantifying mode content in fibers. The principle is to spatially resolve, in a point-by-point fashion, the spectral multi-path interference patterns produced by mode beatings. The imaging setup can either involve a broadband source accompanied by a spatial-scanning system or a tunable laser source accompanied by a CCD camera. For the purposes of this experiment, we chose the latter setup as shown in Fig. 14(a) due to its fast scanning speed and high frequency resolution. Both the tunable laser and the camera scan in sub-seconds and can be easily synchronized by computer control. In addition, the tunable laser supports a fine resolution of 0.0001 nm with a tuning range of 1510–1640 nm. Light coupled from the tunable laser source was launched into approximately 7 m of the fabricated 3-core fiber through free space. The output of the 3-core fiber is imaged onto the camera through a 4-f optical system. A polarizer was added in front of the camera to guarantee a single polarization. During the scanning operation, the laser wavelength was incremented in discrete steps and a mode-interference image was captured by the camera at each step. The measured S^2 results can be expressed as wavelength-interference patterns for every image pixel. An arbitrary excitation can be decomposed into different fiber modes, including the lossy modes which attenuate quickly after a few meters or gentle bends. Because modes travel at different group velocities, if three guided modes are assumed to be excited with amplitudes A, B, C and phase ϕ_a, ϕ_b, ϕ_c, the measured intensity at each pixel location (x, y) would be

$$\begin{aligned} I(\omega)\big|_{(x,y)} &= |A(x,y)\cdot e^{i\phi_a(x,y)}\cdot e^{-i\omega\cdot 0} \\ &\quad + B(x,y)\cdot e^{i\phi_b(x,y)}\cdot e^{-i\omega\cdot\tau_{ab}} \\ &\quad + C(x,y)\cdot e^{i\phi_c(x,y)}\cdot e^{-i\omega\cdot\tau_{ac}}| \\ &= (A^2+B^2+C^2)+2AB \\ &\quad \cdot\cos(\Delta\phi_{ab}-\omega\cdot\tau_{ab}) \\ &\quad + 2AC\cdot\cos(\Delta\phi_{ac}-\omega\cdot\tau_{ac}) \\ &\quad + 2BC\cdot\cos(\Delta\phi_{bc}-\omega\cdot\tau_{bc}), \end{aligned} \tag{4.1}$$

where ω is the angular frequency and τ_{ij} represents the differential group delay between mode i and mode j. An example of a measurement at a particular pixel location is plotted as shown in Fig. 14(b). Using that data, one can extract all the mode information by simply applying a Fourier transform as follows:

$$\begin{aligned} \hat{I}(\tau)\big|_{(x,y)} &= (A^2+B^2+C^2)\cdot\delta(\tau)+\ldots \\ &\quad AB\cdot\left[e^{i\Delta\phi_{ab}}\cdot\delta(\tau+\tau_{ab})+e^{-i\Delta\phi_{ab}}\cdot\delta(\tau-\tau_{ab})\right] \\ &\quad + AC\cdot\left[e^{i\Delta\phi_{ac}}\cdot\delta(\tau+\tau_{ac})+e^{-i\Delta\phi_{ac}}\cdot\delta(\tau-\tau_{ac})\right] \\ &\quad + BC\cdot\left[e^{i\Delta\phi_{bc}}\cdot\delta(\tau+\tau_{bc})+e^{-i\Delta\phi_{bc}}\cdot\delta(\tau-\tau_{bc})\right]. \end{aligned} \tag{4.2}$$

Fig. 14(c) represents the same pixel location after Fourier transform, where every peak corresponds to each mode beating. Therefore, the amplitude, phase, and group delay of the modes can be resolved from the peak strength, phase and locations. Using this method, each mode profile can be extracted from the series of images by performing the Fourier transform on each pixel as shown in the inset of Fig. 14(c).

All the supermodes of the 3-core fiber were obtained using the S^2 imaging method. One difficulty of the experiment is that the mode identification became very complicated due to the large number of fiber modes. Since every peak is the result of the beating of any two modes, the number of the mode-beating peaks scales quadratically with the number of modes. In this experiment, the problem was solved by using intentional offset launching to excite only one dominant mode with a few other modes for each wavelength sweep. Then, multiple excitations were required in order to resolve different modes. Notice that the offset excitation method is selected here for simplicity, while lower loss or more accurate excitation can be achieved by using photonic lanterns [13], [29] or spatial light modulators. S^2 imaging also suffers from the inherent inability to separate degenerate modes, which share same group delays. However, due to the hexagonal shape of the cores in this 3-core fiber,

the degenerate modes actually have a subtle difference in group delay, making it possible to reconstruct each of them separately. Therefore, a total of nine modes supported by the 3-core fiber were successfully reconstructed in both amplitude and phase, as shown in Fig. 15. The first three images are of LP_{01} supermodes, in which the field is slightly better resolved than in those of the LP_{11} supermodes. This is because significantly less power is coupled into the higher-order modes during center or offset excitation. The degenerate higher-order mode images are slightly blurry because their group delay difference is too small to allow them to be clearly differentiated. Nevertheless, the resolved fiber modes are in good agreement with the simulations shown in Fig. 15.

V. Conclusion

We have investigated supermodes in different waveguide array structures based on the weakly-coupled assumption. For coupled single-mode multi-core waveguides, supermodes in multi-ring honeycomb arrangements, which provide the highest mode density per unit cross-sectional area, have been obtained. For coupled few-mode multi-core waveguides, higher-order supermodes have been analyzed for the linear arrays, square lattices and ring arrays. General solutions of LP_{pq} supermodes in those structures of arbitrary sizes are provided. In addition, an experimental observation of higher-order supermodes has been achieved for the first time in a coupled few-mode 3-core fiber. This study enriches the concept of supermodes in coupled multi-core waveguides, which may have potential applications not only in MDM systems [9, 11, 30], but also in other areas related to waveguide optics, such as optical phased arrays [31, 32], beam combining [33, 34] and fiber imaging systems [35, 36].

Appendix A

In order to solve the higher-order supermodes for ring-array structure, diagonalization of the coupled matrix $\boldsymbol{M}$ is the key. It takes two steps as follows. Because each sub-matrix of $\boldsymbol{M}$ has the similar form as the coupled matrix of LP_{01} supermodes, the first step is to utilize the previous solution and diagonalize the sub-matrixes all together. In order to do so, a rank-2N modal matrix is defined as

$$\boldsymbol{P} = \begin{bmatrix} \boldsymbol{Q} & \boldsymbol{0}_N \\ \boldsymbol{0}_N & \boldsymbol{Q} \end{bmatrix}, \tag{A1}$$

where $\boldsymbol{0}_N$ is a N $\times$ N null matrix and $(\boldsymbol{Q})_{lm} = \frac{1}{\sqrt{N}} e^{-i\frac{2\pi l}{N}\cdot m}$ according to Eq. (3.25). $\boldsymbol{P}$ then transforms $\boldsymbol{M}$ into a block matrix composed of diagonal sub-matrixes as below

$$\begin{aligned} \boldsymbol{D} = \ \boldsymbol{P}^{-1}\boldsymbol{M}P &= \begin{bmatrix} \boldsymbol{Q}^{-1}\boldsymbol{M}_{tt}\boldsymbol{Q} & \boldsymbol{Q}^{-1}\boldsymbol{M}_{tn}\boldsymbol{Q} \\ \boldsymbol{Q}^{-1}\boldsymbol{M}_{nt}\boldsymbol{Q} & \boldsymbol{Q}^{-1}\boldsymbol{M}_{nn}\boldsymbol{Q} \end{bmatrix} \\ &= \begin{bmatrix} \boldsymbol{D}_{tt} & \boldsymbol{D}_{tn} \\ \boldsymbol{D}_{nt} & \boldsymbol{D}_{nn} \end{bmatrix}, \end{aligned} \tag{A2}$$

where all the diagonal elements can be calculated

$$(\boldsymbol{D}_{tt})_{l,l} = 2\kappa_{t_1,t_2} \cdot \cos\left(\frac{2\pi l}{N}\right), \tag{A3}$$

$$(\boldsymbol{D}_{tn})_{l,l} = 2i\kappa_{t_1,n_2} \cdot \sin\left(\frac{2\pi l}{N}\right), \tag{A4}$$

$$(\boldsymbol{D}_{nt})_{l,l} = -2i\kappa_{t_1,n_2} \cdot \sin\left(\frac{2\pi l}{N}\right), \tag{A5}$$

$$(\boldsymbol{D}_{nn})_{l,l} = 2\kappa_{n_1,n_2} \cdot \cos\left(\frac{2\pi l}{N}\right), l = 1, 2 \cdots N. \tag{A6}$$

$\boldsymbol{D}$ is a block matrix composed of four diagonal N $\times$ N sub-matrixes, which are commutable with each other. Notice that if $(\boldsymbol{D}_{tn})_{l=l_0} = (\boldsymbol{D}_{nt})_{l=l_0} = 0$, then $(\boldsymbol{D}_{tt})_{l=l_0} = 2\kappa_{t_1,t_2} \cdot \cos\left(\frac{2\pi l_0}{N}\right)$ and $(\boldsymbol{D}_{nn})_{l=l_0} = 2\kappa_{n_1,n_2} \cdot \cos\left(\frac{2\pi l_0}{N}\right)$are eigenvalues already. In addition, a function of a diagonal matrix is still a diagonal matrix, whose elements are the same function of the original matrix elements, i.e., $f(D)_{lm} = f((D)_{ml})$[5]. With these properties, the second step of diagonalization can be operated on $\boldsymbol{D}$ similar to a simple 2 $\times$ 2 matrix of $\begin{bmatrix} a & b \\ c & d \end{bmatrix}$

$$\boldsymbol{\Lambda} = \boldsymbol{R}^{-1}\boldsymbol{D}R. \tag{A7}$$

The eigenvalue matrix is solved as

$$\boldsymbol{\Lambda} = \begin{bmatrix} \frac{1}{2}(\boldsymbol{D}_{tt} + \boldsymbol{D}_{nn} + \boldsymbol{D}_R) & \boldsymbol{0}_N \\ \boldsymbol{0}_N & \frac{1}{2}(\boldsymbol{D}_{tt} + \boldsymbol{D}_{nn} - \boldsymbol{D}_R) \end{bmatrix} \tag{A8}$$

and the modal matrix is

$$\boldsymbol{R} = \begin{bmatrix} \boldsymbol{D}_{tt} - \boldsymbol{D}_{nn} + \boldsymbol{D}_R & \boldsymbol{D}_{tt} - \boldsymbol{D}_{nn} - \boldsymbol{D}_R \\ 2\boldsymbol{D}_{nt} & 2\boldsymbol{D}_{nt} \end{bmatrix}, \tag{A9}$$

in which $\boldsymbol{D}_R = \sqrt{(\boldsymbol{D}_{tt} - \boldsymbol{D}_{nn})^2 + 4\boldsymbol{D}_{tn}\boldsymbol{D}_{nt}}$when $(\boldsymbol{D}_{tn})_{l,l} \neq 0$. Therefore the higher-order supermodes are the row vectors of the matrix $\boldsymbol{R}^{-1}\boldsymbol{P}^{-1}$ where $\boldsymbol{P}^{-1} = \boldsymbol{P}^* = \begin{bmatrix} \boldsymbol{Q}^* & \boldsymbol{0}_N \\ \boldsymbol{0}_N & \boldsymbol{Q}^* \end{bmatrix}$ and $\boldsymbol{R}^{-1} = \begin{bmatrix} 2\boldsymbol{D}_{nt} & \boldsymbol{D}_R - (\boldsymbol{D}_{tt} - \boldsymbol{D}_{nn}) \\ -2\boldsymbol{D}_{nt} & \boldsymbol{D}_R + (\boldsymbol{D}_{tt} - \boldsymbol{D}_{nn}) \end{bmatrix}$.

References

[1] J. K. Butler, D. E. Ackley, and D. Botez, "Coupled-mode analysis of phase-locked injection laser arrays," *Appl. Phys. Lett.*, vol. 44, pp. 293–295, 1984.

[2] E. Kapon, J. Katz, and A. Yariv, "Supermode analysis of phase-locked arrays of semiconductor lasers," *Opt. Lett.*, vol. 9, pp. 125–127, 1984.

[3] A. Hardy and W. Streifer, "Coupled modes of multiwaveguide systems and phased arrays," *J. Lightw. Technol.*, vol. 4, no. 1, pp. 90–99, Jan. 1986.

[4] C. N. Alexeyev, A. V. Volyar, and M. A. Yavorsky, "Linear azimuthons in circular fiber arrays and optical angular momentum of discrete optical vortices," *Phys. Rev. A*, vol. 80, art. no. 063821, 2009.

[5] C. N. Alexeyev, A. V. Volyar, and M. A. Yavorsky, "Energy transfer, orbital angular momentum, and discrete current in a double-ring fiber array," *Phys. Rev. A*, vol. 84, art. no. 063845, 2011.

[6] J. Zhou, "Analytical formulation of super-modes inside multi-core fibers with circularly distributed cores," *Opt. Exp.*, vol. 22, pp. 673–688, 2014.

[7] R. Ryf *et al.*, "Space-division multiplexing over 10 km of three-mode fiber using coherent 6 $\times$ 6 MIMO processing," presented at the IEEE Optical Fiber Communication Conf., Los Angeles, CA, USA, 2011, Paper PDPB10.

[8] B. Neng and L. Guifang, "Adaptive frequency-domain equalization for mode-division multiplexed transmission," *IEEE Photon. Technol. Lett.*, vol. 24, no. 21, pp. 1918–1921, Nov. 2012.
[9] C. Xia, N. Bai, I. Ozdur, X. Zhou, and G. Li, "Supermodes for optical transmission," *Opt. Exp.*, vol. 19, pp. 16653–16664, 2011.
[10] R. Ryf *et al.*, "Impulse response analysis of coupled-core 3-core fibers," presented at the IEEE European Conf. Optical Communication, Amsterdam, The Netherlands, 2012, Paper Mo.1.F.4.
[11] R. Ryf *et al.*, "Space-division multiplexed transmission over 4200 km 3-core microstructured fiber," presented at the IEEE Optical Fiber Communication Conf., Los Angeles, CA, USA, 2012, Paper PDP5C.2.
[12] S. G. Leon-Saval, A. Argyros, and J. Bland-Hawthorn, "Photonic lanterns: A study of light propagation in multimode to single-mode converters," *Opt. Exp.*, vol. 18, pp. 8430–8439, 2010.
[13] S. G. Leon-Saval, A. Argyros, and J. Bland-Hawthorn, "Photonic lanterns," *Nanophotonics*, vol. 2, pp. 429–440, 2013.
[14] C. Xia *et al.*, "Supermodes in strongly-coupled multi-core fibers," presented at the IEEE Opt. Fiber Communication Conf., Anaheim, CA, USA, 2013, Paper OTh3K.5.
[15] J. Zhou, "A non-orthogonal coupled mode theory for super-modes inside multi-core fibers," *Opt Exp.*, vol. 22, pp. 10815–10824, May 5 2014.
[16] Y. Huo and P. K. Cheo, "Analysis of transverse mode competition and selection in multicore fiber lasers," *J. Opt. Soc. Amer. B*, vol. 22, pp. 2345–2349, 2005.
[17] J. Zhou, "Analytical formulation of super-modes inside multi-core fibers with circularly distributed cores," *Opt. Exp.*, vol. 22, pp. 673–688, 2014.
[18] Y.-C. Meng, Q.-Z. Guo, W.-H. Tan, and Z.-M. Huang, "Analytical solutions of coupled-mode equations for multiwaveguide systems, obtained by use of Chebyshev and generalized Chebyshev polynomials," *J. Opt. Soc. Amer. A*, vol. 21, pp. 1518–1528, Aug. 2004.
[19] S. O. Arik and J. M. Kahn, "Coupled-core multi-core fibers for spatial multiplexing," *IEEE Photon. Technol. Lett.*, vol. 25, no. 21, pp. 2054–2057, Nov. 2013.
[20] X. Zhang, X. Zhang, Q. Wang, J. Chang, and G.-D. Peng, "In-phase supermode selection in ring-type and concentric-type multicore fibers using large-mode-area single-mode fiber," *J. Opt. Soc. Amer. A*, vol. 28, pp. 924–933, 2011.
[21] C. Jollivet *et al.*, "Mode-resolved gain analysis and lasing in multi-supermode multi-core fiber laser," *Opt Exp.*, vol. 22, pp. 30377–86, Dec. 1, 2014.
[22] W. H. Ren, Z. W. Tan, and G. B. Ren, "Analytical formulation of supermodes in multicore fibers with hexagonally distributed cores," *IEEE Photon. J.*, vol. 7, no. 1, art. no. 7100311, Feb. 2015.
[23] A. W. Snyder and J. Love, *Optical Waveguide Theory*. New York, NY, USA: Springer, 1983.
[24] K. Okamoto, *Fundamentals of Optical Waveguides*. New York, NY, USA: Academic, 2006.
[25] D. Gloge, "Weakly guiding fibers," *Appl. Opt.*, vol. 10, pp. 2252–2258, 1971.
[26] J. Hudock, N. K. Efremidis, and D. N. Christodoulides, "Anisotropic diffraction and elliptic discrete solitons in two-dimensional waveguide arrays," *Opt. Lett.*, vol. 29, pp. 268–270, Feb 1, 2004.
[27] A. Yariv and P. Yeh, *Photonics: Optical Electronics in Modern Communications*. London, U.K.: Oxford Univ. Press, 2007.
[28] J. Nicholson, A. Yablon, S. Ramachandran, and S. Ghalmi, "Spatially and spectrally resolved imaging of modal content in large-mode-area fibers," *Opt. Exp.*, vol. 16, pp. 7233–7243, 2008.
[29] S. Leon-Saval, T. Birks, J. Bland-Hawthorn, and M. Englund, "Multimode fiber devices with single-mode performance," *Opt. Lett.*, vol. 30, pp. 2545–2547, 2005.
[30] S. O. Arik and J. M. Kahn, "Coupled-core multi-core fibers for spatial multiplexing," *IEEE Photon. Technol. Lett.*, vol. 25, no. 21, pp. 2054–2057, Nov. 2013.
[31] L. Li *et al.* "Phase locking and in-phase supermode selection in monolithic multicore fiber lasers," *Opt. Lett.*, vol. 31, pp. 2577–2579, 2006.
[32] J. Sun, E. Timurdogan, A. Yaacobi, E. S. Hosseini, and M. R. Watts, "Large-scale nanophotonic phased array," *Nature*, vol. 493, pp. 195–199, 2013.
[33] E. J. Bochove and S. Shakir, "Analysis of a spatial-filtering passive fiber laser beam combining system," *IEEE J. Sel. Topics Quantum Electron.*, vol. 15, no. 2, pp. 320–327, Mar./Apr. 2009.
[34] C. J. Corcoran and F. Durville, "Passive phasing in a coherent laser array," *IEEE J. Sel. Topics Quantum Electron.*, vol. 15, no. 2, pp. 294–300, Mar./Apr. 2009.
[35] D. Kim *et al.*, "Toward a miniature endomicroscope: Pixelation-free and diffraction-limited imaging through a fiber bundle," *Opt. Lett.*, vol. 39, pp. 1921–1924, 2014.
[36] K. L. Reichenbach and C. Xu, "Numerical analysis of light propagation in image fibers or coherent fiber bundles," *Opt. Exp.*, vol. 15, pp. 2151–2165, 2007.

Cen Xia received the B.S. degree in optical engineering from Zhejiang University, Zhejiang, China, in 2009 and is currently working toward the Ph.D. degree in CREOL, University of Central Florida, Orlando, FL, USA. Her research interests include space division multiplexing and fiber design and characterization. She has published 15 journal and conference papers (including 11 first-author papers) and received best student paper award (first prize) in Asia Communications and Photonics Conference.

M. Amin Eftekhar received the B.S. degree from the Shiraz University of Technology, Modarres Boulevard, Iran, in 2009 and the M.S. degree from the University of Tehran, Tehran, Iran, in 2012 both in electrical engineering. In 2013, he joined CREOL, University of Central Florida and he is currently working toward the Ph.D. degree. His research interests include linear and nonlinear optical beam interactions, synthetic optical materials, optical solitons, and quantum electronics.

Rodrigo Amezcua Correa received the B.Eng. degree from the National Autonomous University of Mexico, Mexico, in 2002, and the Ph.D. degree from the Optoelectronics Research Centre, University of Southampton, Southampton, U.K., in 2008. He then joined the Centre for Photonics and Photonic Materials at Bath University as a Postdoctoral Researcher in the field of fiber optics. In 2011, he joined the College of Optics and Photonics, University of Central Florida, as a Research Assistant Professor where his research focuses on fiber optics and fiber optics components.

Jose Enrique Antonio-Lopez received the B.S. degree in electronic engineering form the Salina Cruz institute of Technology, Oaxaca, Mexico, in 2004 and the M.S. and Ph.D. degrees in optics from the National Institute for Astrophysics, Optics and Electronics, Puebla, Mexico, in 2008 and 2012 respectively. He is currently working as a Postdoctoral Fellow in CREOL, the College in Optics and Photonics at the University of Central Florida, Orlando, FL, USA.

His research interest includes the development of novel fabrication processes for microstructured optical fiber such as hollow core fibers, multicore fibers, large-pitch double-clad optical photonics crystal fibers, and also special optical fibers for medical applications. He also works in the fabrication and testing of all-fiber fiber optics devices for telecommunications and optical sensing applications.

Axel Schülzgen, photograph and biography not available at the time of publication.

Demetrios Christodoulides received the Ph.D. degree from Johns Hopkins University, Baltimore, MD, USA, in 1986 and he subsequently joined Bellcore as a PostDoctoral Fellow at Murray Hill. He is the Cobb Family Endowed Chair and the Pegasus Professor of Optics at CREOL—the College of Optics and Photonics of the University of Central Florida, Orlando, FL, USA. Between 1988 and 2002, he was with the faculty of the Department of Electrical Engineering, Lehigh University. His research interests include linear and nonlinear optical beam interactions, synthetic optical materials, optical solitons, and quantum electronics. His research initiated new innovation within the field, including the discovery of optical discrete solitons, Bragg and vector solitons in fibers, nonlinear surface waves, and the discovery of self-accelerating optical (Airy) beams. He has authored and co-authored more than 300 papers. He is a Fellow of the Optical Society of America and the American Physical Society. In 2011, he received the R.W. Wood Prize of OSA.

Guifang Li (M'94–SM'06–F'13) received the Ph.D. degree from The University of Wisconsin at Madison, Madison, WI, USA. He was the Director of the NSF IGERT program in Optical Communications and Networking at the University of Central Florida, Orlando, FL, USA. He received the NSF CAREER Award and the Office of Naval Research Young Investigator Award. He is a Fellow of IEEE, The Optical Society, and SPIE. He is the Deputy Editor for Optics Express, Overseas Editor-in-Chief of Frontiers of Optoelectronics, and an Associate Editor for Photonics Technology Letters, and the Chinese Optics Letters.